IEEE Access
Multidisciplinary ⋮ Rapid Review ⋮ Open Access Journal

Received February 14, 2020, accepted February 26, 2020, date of publication March 9, 2020, date of current version March 18, 2020.

Digital Object Identifier 10.1109/ACCESS.2020.2979223

Novel Lyapunov-Based Autonomous Controllers for Quadrotors

JAI RAJ[1], KRISHNA S. RAGHUWAIYA[2], AND JITO VANUALAILAI[1]
[1]School of Computing, Information, and Mathematical Sciences, The University of the South Pacific, Private Mail Bag, Laucala Campus, Suva, Fiji
[2]School of Education, The University of the South Pacific, Private Mail Bag, Laucala Campus, Suva, Fiji

Corresponding author: Jito Vanualailai (jito.vanualailai@usp.ac.fj)

ABSTRACT In this paper, we look into the dynamic motion planning and control of an unmanned aerial vehicle, namely, the quadrotor, governed by its dynamical equations. It is shown for the first time that the Direct or the Second Method of Lyapunov is an effective tool to derive a set of continuous nonlinear control laws that not only provide smooth trajectories from a designated initial position to a designated target, but also continuously minimise the roll and pitch of the quadrotor en route to its targets. The latter successfully addresses the challenging problem of a quadrotor autonomously transporting valuable and fragile payloads safely to the designated target. Computer simulations are used to illustrate the effectiveness of the proposed control laws.

INDEX TERMS Artificial potential field, Lyapunov-based control scheme, quadrotor, stability, UAV.

I. INTRODUCTION

The development and deployment of autonomous flying vehicles have gained enormous interests from the commercial, industrial and scholarly sectors in recent years because of the wide range of novel applications that have opened up with their uses. The research on unmanned aerial vehicles (UAVs) has opened the way to several complex and highly prominent applications for both military and civilian markets, including rescue missions, fire-fighting, delivery, health, maintenance, surveillance and transportation [1]–[4]. UAVs can help save lives during natural and man-made disasters, locate stranded and injured people, and assess ongoing threats without risking the safety of rescue teams. They can be operated in dangerous environments with relatively low cost and without putting the human lives at risk. With climate change affecting the low-lying areas and increasing the frequency of severe cyclones and bush fires, UAVs will play a very crucial role for disaster management teams. In addition, UAVs will be very useful in agriculture management and surveillance for the protection of flora and fauna.

Among the UAVs, the quadrotors have attracted particular attention by researchers, given their advantages over other vertical take-off and landing UAVs. Its reduced mechanical complexity, payload augmentation, gyroscopic effect reduction, useful flight modes, variety of sizes and minimum damage in case of collision are the features that make the quadrotors more advantageous over other UAVs [2]–[5]. The quadrotor relies on fixed pitch rotors and uses the variation in motor speed for vehicle control; hence it does not have complex mechanical control linkages [6]. However, these advantages also come at a certain cost, given that controlling a quadrotor is a complex task. This makes the flight control a challenging problem because of the coupled dynamics which are highly nonlinear, constraints, under-actuated design configuration and several uncertainties that are encountered during flight [7], [8]. During flight, the quadrotors are always subjected to various disturbances and uncertainties in the forms of parametric perturbations, noise and wind gusts [9]. Thus, the question on how to achieve high-performance and robust control of quadrotors is an interesting and valuable task, still yet a challenging problem. Nonetheless, this has lead to the design and evaluation of a broad range of control techniques to improve the flight performance of quadrotors.

Numerous research studies have examined the attitude and position control design and implementation to retain satisfactory performance operation. Some of the several control algorithms proposed in the literature includes proportional integral derivative (PID) [10], [11], linear quadratic regulator (LQR) [8], [10], [12], sliding mode control [13], [14], H_∞ [15], backstepping control [9], fuzzy logic [16], and visual-based techniques [17]. Another interesting

The associate editor coordinating the review of this manuscript and approving it for publication was Ning Sun.

methodology by Chen and Sun in 2019 [18], which generally deals with the control of underactuated systems that can treat various system constraints, could be used to control quadrotors.

In this paper, we introduce a Lyapunov-based control scheme (LbCS) which is an Artificial Potential Field (APF) method to extract control laws that govern the control and stability of quadrotors [19]–[22]. The APF method was pioneered by Khatib [23] in 1986 to address the findpath problem involving manipulators and autonomous robots. Since then, the method has found wide applications in the field of robotics. The algorithms in the APF method tend to use physical analogies to establish repulsive poles around the obstacles and attractive poles around goals. The workspace is inundated with negative and positive fields, with the direction of motion facilitated via the notion of steepest decent [24]. The attractive and repulsive forces control the motion of the robot. As the mobile robot approaches the obstacles, it will experience high repulsive force so the robot will move towards a low potential, which could lead towards the target for the robotic system.

Although the Lyapunov method has already been utilised in the control and stability of quadrotors [25]–[28] and other mechanical systems [18], [29]–[31], the approach has been mainly in the traditional manner of ensuring only that the mechanical system is stable after the controllers have been designed using different algorithms or methods. Our method of applying the Second Method of Lyapunov differs markedly in the new field. Specifically, the proposed method uses the Second Method of Lyapunov directly by substituting the ordinary differential equations that govern the quadrotor system into the time-derivative of the Lyapunov-like function and then designing the controllers such that the time-derivative of the Lyapunov-like function is negative definite and satisfies the stability criteria of the Second Method of Lyapunov. This is different from the bulk of the Lyapunov-based methods that are used now. These methods propose a certain form of the controllers, for instance, using PID, LQR, sliding mode control, backstepping control, fuzzy logic, and visual-based techniques, and then use the Second Method of Lyapunov to verify that the system is stable. These methods are used more for trajectory tracking rather than hovering maneuvers of the quadrotor. In our case, our controllers address the latter issue. Also, our approach is different from other motion planning and control schemes from literature which do not specifically take into account system constraints as components of the controllers [21], [32], [33].

The organisation of this article is as follows. Section II presents the dynamic model of the quadrotor and the objective of the paper. In Section III, the attractive and the repulsive potential field functions are constructed. In Section IV, a Lyapunov-like function whose components are the attractive and repulsive field functions is constructed. The nonlinear control laws for the quadrotor model are then extracted from the Lyapunov-like function. In Section V, the stability of the quadrotor model is analysed via a theorem by Yoshizawa.

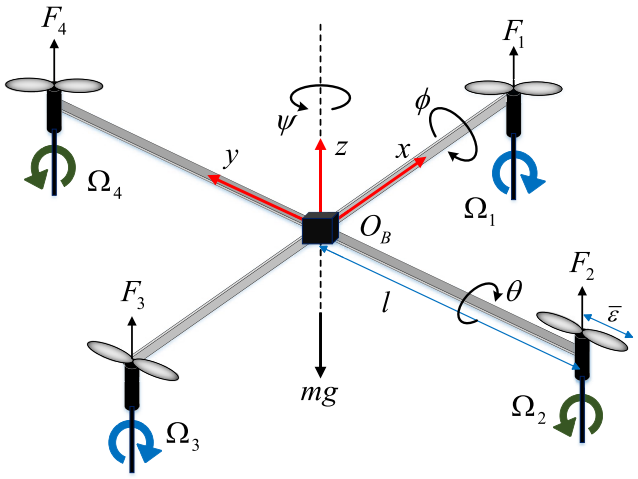

FIGURE 1. The schematic structural configuration of a quadrotor UAV with body and earth reference frames.

In Section VI, the flight control for the quadrotor model is simulated and the results are presented to verify the effectiveness and the superiority of the proposed robust control laws. Finally, the conclusions and future work are given in Section VII.

II. QUADROTOR DYNAMIC MODEL

A quadrotor has four rotors, each comprising of a motor coupled with a propeller to create thrust, F_i, $i = 1, 2, 3, 4$, to provide the aircraft lift. Two of the rotors (2 and 4) makes the propellers rotate in clockwise direction while the other two rotors (1 and 3) generate a balancing torque with a counter-clockwise propeller rotation (see Fig. 1). The roll (ϕ), pitch (θ), yaw (ψ) and up-thrust actions are controlled by changing the thrusts of the rotors. The cooperative rotations of the four rotors ensures the motion and control performance of the quadrotor. The vertical lift is controlled by collectively increasing or decreasing the rotational speed of the four rotors. The differential speed of the rotors (1 and 3) and (2 and 4) results in the pitch and roll motions, which contributes to the longitudinal x and y motions respectively. The difference of counter-torques generated by each of the propellers results in yaw motion. The derivation of the equations of motion for a dynamic model that describes the attitude and position of the quadrotor requires two reference frames, namely the body-fixed frame denoted as B and the earth-fixed frame denoted as E.

Using the classical yaw, pitch and roll Euler angles applied in aeronautical applications, the rotation matrix can be expressed as

$$R_r = \begin{bmatrix} c\theta c\psi & s\phi s\theta c\psi - c\phi s\psi & c\phi s\theta c\psi + s\phi s\psi \\ c\theta s\psi & s\phi s\theta s\psi + c\phi c\psi & c\phi s\theta s\psi - s\phi c\psi \\ -s\theta & s\phi c\theta & c\phi c\theta \end{bmatrix} \quad (1)$$

and the transformation matrix is defined as

$$R_t = \begin{bmatrix} 1 & 0 & -s\theta \\ 0 & c\phi & c\theta s\psi \\ 0 & -s\phi & c\phi c\theta \end{bmatrix} \tag{2}$$

where $s(\cdot)$ and $c(\cdot)$ are abbreviations for $\sin(\cdot)$ and $\cos(\cdot)$. The dynamic model of the quadrotor is derived utilising the Euler-Lagrange approach with the following assumptions [10], [34]:

- The structure of the quadrotor is rigid and symmetrical.
- The centre of mass and the origin of the body-fixed frame coincides.
- The propellers are rigid.
- The thrust and drag forces are proportional to the square of the propellers speed.

As shown in [13], a simplified dynamic model of the quadrotor can be expressed by the following nonlinear differential equations:

$$\left.\begin{aligned} \ddot{x} &= \frac{U_1}{m}\left(\cos\phi\sin\theta\cos\psi + \sin\phi\sin\psi\right) - \kappa_1\frac{\dot{x}}{m}, \\ \ddot{y} &= \frac{U_1}{m}\left(\cos\phi\sin\theta\sin\psi - \sin\phi\cos\psi\right) - \kappa_2\frac{\dot{y}}{m}, \\ \ddot{z} &= \frac{U_1}{m}\cos\phi\cos\theta - g - \kappa_3\frac{\dot{z}}{m}, \\ \ddot{\phi} &= \frac{l}{I_x}U_2 - l\kappa_4\frac{\dot{\phi}}{I_x}, \\ \ddot{\theta} &= \frac{l}{I_y}U_3 - l\kappa_5\frac{\dot{\theta}}{I_y}, \\ \ddot{\psi} &= \frac{1}{I_z}U_4 - \kappa_6\frac{\dot{\psi}}{I_z}, \end{aligned}\right\} \tag{3}$$

where (x, y, z) represents the real-time position of quadrotor in the earth-frame, (ϕ, θ, ψ) are the three Euler angles, g is the gravitational acceleration, m is the total mass of the quadrotor structure, l is the half length of the quadrotor, $I_{x,y,z}$ symbolises the moments of inertia with respect to the respective x, y and z axes, κ_is are the drag coefficients, U_is are the virtual control inputs defined as follows:

$$\left.\begin{aligned} U_1 &= \sqrt{U_{1x}^2 + U_{1y}^2 + U_{1z}^2} \\ &= K_F\left(\Omega_1^2 + \Omega_2^2 + \Omega_3^2 + \Omega_4^2\right), \\ U_2 &= K_F\left(\Omega_3^2 - \Omega_1^2\right), \\ U_3 &= K_F\left(\Omega_2^2 - \Omega_4^2\right), \\ U_4 &= K_M\left(\Omega_1^2 - \Omega_2^2 + \Omega_3^2 - \Omega_4^2\right), \end{aligned}\right\} \tag{4}$$

where K_F is the force constant, K_M is a torque constant and Ω_is are the speed of the rotors and can be considered as the real control inputs to the system. Since the drag is very small at low speeds, the drag terms can be considered as small disturbances to the system.

Now, the quadrotor model has six outputs $(x, y, z, \phi, \theta, \psi)$ while only four independent inputs (U_1, U_2, U_3, U_4) are available; therefore the quadrotor is a typical higher-order under-actuated system. To solve this problem, we introduce new control inputs to replace U_1. There are the three components of U_1, namely, U_{1x}, U_{1y} and U_{1z} which encompass the x, y and z translational components of the quadrotor. With this modification, the quadrotor dynamic model now consists of an angular rotational subsystem and a linear translational subsystem, as shown in Fig. 2. The dynamics of the rotational system, the angles and their time derivatives do not depend on the translational components. However the translational components depend on roll, pitch and yaw, and not on the angular velocities. In general, the yaw, pitch and roll are acquired from the angular rotational system and together with U_{1x}, U_{1y} and U_{1z}, they become inputs into the translation subsystem. Therefore, the problem of the under-actuation inherent in the quadrotor system can be solved by introducing the control inputs U_{1x}, U_{1y} and U_{1z} to replace U_1.

Now, let the state vector for the quadrotor model be

$$\mathbf{x} = (x, y, z, \phi, \theta, \psi, v, w, u, q, p, r) \in \mathbb{R}^{12}. \tag{5}$$

Then a system of first-order differential equations (ODEs) for the quadrotor model is

$$\left.\begin{aligned} \dot{x} &= v, \\ \dot{y} &= w, \\ \dot{z} &= u, \\ \dot{v} &= \frac{U_{1x}}{m}\left(\cos\phi\sin\theta\cos\psi + \sin\phi\sin\psi\right) - \kappa_1\frac{v}{m}, \\ \dot{w} &= \frac{U_{1y}}{m}\left(\cos\phi\sin\theta\sin\psi - \sin\phi\cos\psi\right) - \kappa_2\frac{w}{m}, \\ \dot{u} &= \frac{U_{1z}}{m}\cos\phi\cos\theta - g - \kappa_3\frac{u}{m}, \\ \dot{\phi} &= q, \\ \dot{\theta} &= p, \\ \dot{\psi} &= r, \\ \dot{q} &= \frac{l}{I_x}U_2 - l\kappa_4\frac{q}{I_x}, \\ \dot{p} &= \frac{l}{I_y}U_3 - l\kappa_5\frac{p}{I_y}, \\ \dot{r} &= \frac{1}{I_z}U_4 - \kappa_6\frac{r}{I_z}. \end{aligned}\right\} \tag{6}$$

With this system of first-order ODEs, it is now easier to construct the six controllers using the Direct Method of Lyapunov. Hence, our objective in this paper is to construct the autonomous control laws $U_{1x}, U_{1y}, U_{1z}, U_2, U_3$ and U_4 for the quadrotor governed by (6) that will allow it to move from an initial configuration to its final destination. If $(Z_1, Z_2, Z_3) := (X_E, Y_E, Z_E)$ and the length of a radiating blade is $\bar{\varepsilon} > 0$, then we can precisely defined the quadrotor as follows:

Definition 1: The quadrotor is a sphere with centre (x, y, z) and radius $r_Q := l + \bar{\varepsilon}$. That is, it is the set

$$\mathcal{A} = \left\{(Z_1, Z_2, Z_3) \in \mathbb{R}^3 : (Z_1 - x)^2 + (Z_2 - y)^2 + (Z_3 - z)^2 \leq r_Q^2\right\}.$$

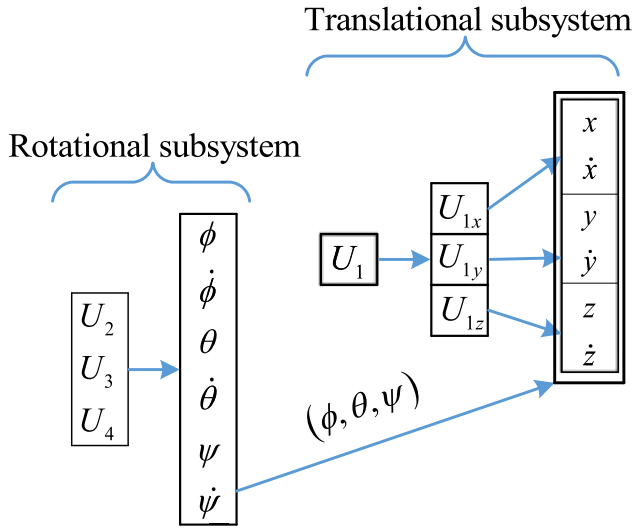

FIGURE 2. The relationship between the rotational and translational systems. Modified from [3].

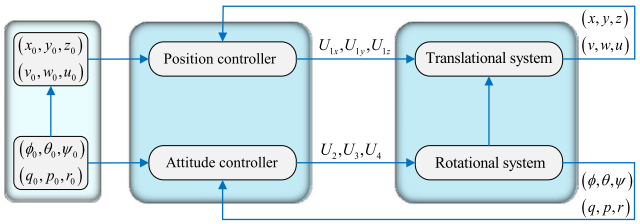

FIGURE 3. Control architecture of the LbCS for the quadrotor system.

III. APF FUNCTIONS FOR AVOIDANCE AND ATTRACTION

In this section, we formulate collision-free trajectories of system (6) using the APF method. The principle notion that governs the APF method is finding a function that represents the energy of the system, such as the Lyapunov function and generating a force so that the energy of the system is minimized and reach the minimum value, preferably only at the target configuration. The energy of the system is mathematically treated as the total potential. We design the control inputs $U_{1x}, U_{1y}, U_{1z}, U_2, U_3$ and U_4, such that $\mathcal{A}$ will navigate safely and reach a neighborhood of its target. To obtain a feasible solution, we utilise the APF functions in the LbCS to design the new controllers. The APFs will be the attractive APFs for convergence and the repulsive APFs to ensure that the quadrotor functions within its constraints. In order to demonstrate the LbCS design for the quadrotor system intuitively, the control architecture is illustrated in Fig. 3. We begin by describing precisely the target and dynamic constraints of $\mathcal{A}$.

A. ATTRACTIVE POTENTIAL FIELD FUNCTIONS

1) ATTRACTION TO TARGET AND POSTURE STABILISATION

To initiate the movement of $\mathcal{A}$, we affix a target for $\mathcal{A}$ to reach after some time $t > 0$. It is defined as follows:

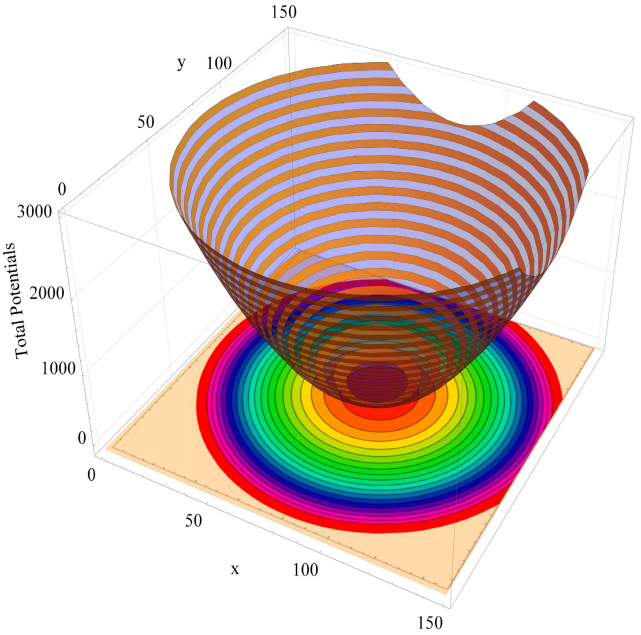

FIGURE 4. The attractive potential fields generated using the target attractive function, equation (7), without the z-component of the target.

Definition 2: The designated target for $\mathcal{A}$ is a sphere with centre (τ_1, τ_2, τ_3) and radius r_τ. That is, it is the set

$$T = \left\{(Z_1, Z_2, Z_3) \in \mathbb{R}^3 : (Z_1 - \tau_1)^2 + (Z_2 - \tau_2)^2 + (Z_3 - \tau_3)^2 \leq r_\tau^2\right\}.$$

Intuitively, we want to have a yardstick that measures, at time $t > 0$, the centre of $\mathcal{A}$ to its target destination (τ_1, τ_2, τ_3) and the rate at which it approaches or moves away from (τ_1, τ_2, τ_3). Hence, for attraction to the target, we consider

$$V_1(\mathbf{x}) = \frac{1}{2}\left[(x - \tau_1)^2 + (y - \tau_2)^2 + (z - \tau_3)^2\right]. \quad (7)$$

The function $V_1(\mathbf{x})$ will serve as an attractive potential function, attracting $\mathcal{A}$ to its designated target. An illustration of the total potentials for the target attraction function is shown in Figure 4, generated over a workspace $0 < x, y < 150$ for $\mathcal{A}$. The disk-shaped target for the quadrotor is fixed at $(\tau_1, \tau_2) = (80, 80)$ with a radius of $r_\tau = 1$.

2) QUADROTOR POSTURE STABILISATION

The goal is to ensure that quadrotor stabilise itself while en route to its target. That is, we want the quadrotor to have a low degree of tilting in roll and pitch so that it maintains its near-to-horizontal orientation while in motion. Subsequently, we want the endpoints 1 and 4 of $\mathcal{A}$ (see Fig. 1) to have and maintain an angular displacement of zero. To ensure that the endpoint 1 has a near-to-horizontal orientation, we use the vector

$$(x, y, z)^T + lR_r(1, 0, 0)^T = (x + lc\theta c\psi, y + lc\theta s\psi, z - ls\theta)^T.$$

Similarly, for the endpoint 4, we consider the vector

$$(x, y, z)^T + lR_r(0, 1, 0)^T$$
$$= (x+ls\phi s\theta c\psi - lc\phi s\psi, y+lc\phi c\psi + ls\phi s\theta s\psi, z+ls\phi c\theta)^T.$$

That is, generally, for the endpoints to achieve a near-to-horizontal orientation, the following operations are carried out

$$(x, y, z)^T + lR_r\left((1, 0, 0)^T, (0, 1, 0)^T, (0, 0, 1)^T\right).$$

For our case, it is sufficient to consider a stabilisation function of the form

$$V_2(\mathbf{x}) = \frac{1}{2}\begin{bmatrix} (x + lc\theta c\psi - \tau_4)^2 \\ +(y + lc\theta s\psi - \tau_5)^2 \\ +(z - ls\theta - \tau_6)^2 \\ +(x + ls\phi s\theta c\psi - lc\phi s\psi - \tau_7)^2 \\ +(y + lc\phi c\psi + ls\phi s\theta s\psi - \tau_8)^2 \\ +(z + ls\phi c\theta - \tau_9)^2 \end{bmatrix}, \quad (8)$$

where $\tau_4 = \tau_1 + l$, $\tau_5 = \tau_2$, $\tau_6 = \tau_3$, $\tau_7 = \tau_1$, $\tau_8 = \tau_2 + l$ and $\tau_9 = \tau_3$.

3) VELOCITIES OF THE QUADROTOR

While equation (7) is a measure of the distance between $\mathcal{A}$ and its target V_1, it can also be treated as a measure of convergence with the inclusion of the velocity components (angular and translation). Hence, to have a complete form of the attractive potential field function of the quadrotor, we consider an additional function for the velocity components:

$$V_3(\mathbf{x}) = \frac{1}{2}\left[v^2 + w^2 + u^2 + q^2 + p^2 + r^2\right], \quad (9)$$

where v, w, u are the translational velocities and q, p, r are the angular velocities. Then the total attractive potential field function of the quadrotor is

$$V(\mathbf{x}) = \sum_{i=1}^{3} V_i(\mathbf{x}). \quad (10)$$

B. REPULSIVE POTENTIAL FIELD FUNCTIONS

There is a necessity to impose constraints on certain variables to induce the desired performance for quadrotors with payloads. In this section, we show how ghost or artificial obstacles can aid in this. Artificial obstacles are simply mechanical and workspace constraints that have to be recognised by the controllers which then induce an avoidance response by the quadrotor.

1) MODULUS BOUND ON THE ANGLES

Unless one requires acrobatic vehicle configurations [35], the pitch, roll and yaw of $\mathcal{A}$ must be bounded to prevent the quadrotor UAV from flipping over. The constraints imposed on the pitch, roll and yaw are: (i)

1) $|\phi| \leq \phi_{\max}$, where ϕ_{max} is the maximum pitching angle. To avoid the quadrotor from having a vertical pitch, we let $0 < \phi_{\max} < \pi/2$;
2) $|\theta| \leq \theta_{\max}$, where θ_{max} is the maximum rolling angle. To avoid the quadrotor from having a vertical-sideways roll, we let $0 < \theta_{\max} < \pi/2$;
3) $|\psi| \leq \psi_{\max}$, where ψ_{max} is the maximum yawing angle. To avoid the quadrotor from yawing about its origin, we let $0 < \psi_{\max} < \pi$. The constraint on the yaw angle can be very useful in applications such as when a camera is onboard the quadrotor vehicle and needs to be targeted towards a particular region.

A systematic way these dynamic constraints can factored into the motion planners and control schemes of the quadrotor is by constructing artificial obstacles and then avoiding them to achieve the desired outcome. For each of the dynamic constraints, we construct a corresponding artificial obstacle:

$$AO_1 = \{\phi \in \mathbb{R} : |\phi| < \phi_{\max}\},$$
$$AO_2 = \{\theta \in \mathbb{R} : |\theta| < \theta_{\max}\},$$
$$AO_3 = \{\psi \in \mathbb{R} : |\psi| < \psi_{\max}\}.$$

Then for the avoidance of these artificial obstacles, we consider the following obstacle avoidance functions [36], [37]:

$$S_1(\mathbf{x}) = \frac{1}{2}(\phi_{\max} - \phi)(\phi_{\max} + \phi), \quad (11)$$
$$S_2(\mathbf{x}) = \frac{1}{2}(\theta_{\max} - \theta)(\theta_{\max} + \theta), \quad (12)$$
$$S_3(\mathbf{x}) = \frac{1}{2}(\psi_{\max} - \psi)(\psi_{\max} + \psi). \quad (13)$$

Over the sets AO_i, $i = 1, 2, 3$, these functions are positive.

2) MODULUS BOUND ON THE VELOCITIES

Translational and angular velocities of the quadrotors must also be restricted due to safety reasons. These are dynamical constraints. (i)

1) $|v| \leq v_{\max}$, where $v_{\max}$ is the *maximum achievable speed* of the of the quadrotor aircraft in the x direction;
2) $|w| \leq w_{\max}$, where $w_{\max}$ is the *maximum achievable speed* of the of the quadrotor aircraft in the y direction;
3) $|u| \leq u_{\max}$, where $u_{\max}$ is the *maximum achievable speed* of the of the quadrotor aircraft in the z direction;
4) $|q| \leq q_{\max}$, where $q_{\max}$ is the maximum roll rate;
5) $|p| \leq p_{\max}$, where $p_{\max}$ is the maximum pitch rate;
6) $|r| \leq r_{\max}$, where $r_{\max}$ is the maximum yaw rate.

The corresponding artificial obstacles are:

$$AO_4 = \{v \in \mathbb{R} : |v| < v_{\max}\},$$
$$AO_5 = \{w \in \mathbb{R} : |w| < w_{\max}\},$$
$$AO_6 = \{u \in \mathbb{R} : |u| < u_{\max}\},$$
$$AO_7 = \{q \in \mathbb{R} : |q| < q_{\max}\},$$
$$AO_8 = \{p \in \mathbb{R} : |p| < p_{\max}\},$$
$$AO_9 = \{r \in \mathbb{R} : |r| < r_{\max}\}.$$

For the avoidance of these artificial obstacles, we adopt the following obstacle avoidance functions:

$$D_1(\mathbf{x}) = \frac{1}{2}(v_{\max} - v)(v_{\max} + v), \quad (14)$$

$$D_2(\mathbf{x}) = \frac{1}{2}(w_{\max} - w)(w_{\max} + w), \quad (15)$$

$$D_3(\mathbf{x}) = \frac{1}{2}(u_{\max} - u)(u_{\max} + u), \quad (16)$$

$$D_4(\mathbf{x}) = \frac{1}{2}(q_{\max} - q)(q_{\max} + q), \quad (17)$$

$$D_5(\mathbf{x}) = \frac{1}{2}(p_{\max} - p)(p_{\max} + p), \quad (18)$$

$$D_6(\mathbf{x}) = \frac{1}{2}(r_{\max} - r)(r_{\max} + r). \quad (19)$$

IV. DESIGN OF THE NONLINEAR CONTROLLERS

In this section, the nonlinear control laws for system (6) will be designed using LbCS.

A. A LYAPUNOV-LIKE FUNCTION

Introduce the following *control/tuning parameters*: (i)

1) $\xi_s > 0$, $s = 1, \ldots, 3$, for the avoidance of sth artificial obstacles from the dynamic constraints of the angles (see Subsection III-B.1);
2) $\gamma_d > 0$, $d = 1, \ldots, 6$, for the avoidance of the dth artificial obstacles from dynamic constraints of the translational and rotational velocities (see Subsection III-B.2).

Then consider, as a tentative Lyapunov-like function for system (6) with two components, namely, the attractive and repulsive potential field functions, the following:

$$L(\mathbf{x}) = V(\mathbf{x}) + G(\mathbf{x})\left(\sum_{s=1}^{3}\frac{\xi_s}{S_s(\mathbf{x})} + \sum_{d=1}^{6}\frac{\gamma_d}{D_d(\mathbf{x})}\right), \quad (20)$$

where $G(\mathbf{x})$ is an auxiliary function meant to have L behave like a Lyapunov function near the vicinity of the target where we want $L \approx 0$:

$$G(\mathbf{x}) = \frac{1}{2}\left[(x-\tau_1)^2 + (y-\tau_2)^2 + (z-\tau_3)^2\right] + \epsilon^2. \quad (21)$$

Here, $\epsilon \in \mathbb{R}$, $\epsilon > 0$ will be chosen to be sufficiently small.

We note that L is positive over the domain:

$$\mathbb{D}(L) = \left\{\mathbf{x} \in \mathbb{R}^{12} : S_s(\mathbf{x}) > 0, s = 1, 2, 3 \text{ and } D_d(\mathbf{x}) > 0, d = 1, \ldots, 6\right\}.$$

B. NONLINEAR CONTROLLERS

The feedback control laws for the dynamic system is extracted by finding the time derivative of the various components of $L(\mathbf{x})$ along a solution of dynamic system (6) and force it to be at least semi-negative definite. Upon suppressing $\mathbf{x}$, the time derivative of $L(\mathbf{x})$, equation (20) is

$$\dot{L}_{(6)}(\mathbf{x}) = f_1 v + f_2 w + f_3 u + f_4 v\dot{v} + f_5 w\dot{w} + f_6 u\dot{u} + g_1 q + g_2 p + g_3 r + g_4 q\dot{q} + g_5 p\dot{p} + g_6 r\dot{r}, \quad (22)$$

where

$$f_1 = \left(1 + \sum_{s=1}^{3}\frac{\xi_s}{S_s} + \sum_{d=1}^{6}\frac{\gamma_d}{D_d}\right)(x-\tau_1) + (x + lc\theta c\psi - \tau_4) + (x + ls\phi s\theta c\psi - lc\phi s\psi - \tau_7),$$

$$f_2 = \left(1 + \sum_{s=1}^{3}\frac{\xi_s}{S_s} + \sum_{d=1}^{6}\frac{\gamma_d}{D_d}\right)(y-\tau_2) + (y + lc\theta s\psi - \tau_5) + (y + lc\phi c\psi + ls\phi s\theta s\psi - \tau_8),$$

$$f_3 = \left(1 + \sum_{s=1}^{3}\frac{\xi_s}{S_s} + \sum_{d=1}^{6}\frac{\gamma_d}{D_d}\right)(z-\tau_3) + (z - ls\theta - \tau_6) + (z + ls\phi c\theta - \tau_9),$$

$$f_4 = 1 + \frac{\gamma_1 G}{D_1^2}, \quad f_5 = 1 + \frac{\gamma_2 G}{D_2^2}, \quad f_6 = 1 + \frac{\gamma_3 G}{D_3^2},$$

$$g_1 = \begin{pmatrix} l(x + ls\phi s\theta c\psi - lc\phi s\psi - \tau_7)\, c\phi s\theta c\psi \\ +l(x + ls\phi s\theta c\psi - lc\phi s\psi - \tau_7)\, s\phi s\psi \\ -l(y + lc\phi c\psi + ls\phi s\theta s\psi - \tau_8)\, s\phi c\psi \\ +l(y + lc\phi c\psi + ls\phi s\theta s\psi - \tau_8)\, c\phi s\theta s\psi \\ +l(z + ls\phi c\theta - \tau_9)\, c\phi c\theta \end{pmatrix} + \frac{\xi_1 G}{S_1^2}\phi,$$

$$g_2 = \begin{pmatrix} -l(x + lc\theta c\psi - \tau_4)\, s\theta c\psi \\ -l(y + lc\theta s\psi - \tau_5)\, s\theta s\psi - l(z - ls\theta - \tau_6)\, c\theta \\ +l(x + ls\phi s\theta c\psi - lc\phi s\psi - \tau_7)\, s\phi c\theta c\psi \\ +l(y + lc\phi c\psi + ls\phi s\theta s\psi - \tau_8)\, s\phi c\theta s\psi \\ -l(z + ls\phi c\theta - \tau_9)\, s\phi s\theta \end{pmatrix} + \frac{\xi_2 G}{S_2^2}\theta,$$

$$g_3 = \begin{pmatrix} -l(x + lc\theta c\psi - \tau_4)\, c\theta s\psi \\ +l(y + lc\theta s\psi - \tau_5)\, c\theta c\psi \\ -l(x + ls\phi s\theta c\psi - lc\phi s\psi - \tau_7)\, s\phi s\theta s\psi \\ -l(x + ls\phi s\theta c\psi - lc\phi s\psi - \tau_7)\, c\phi c\psi \\ -l(y + lc\phi c\psi + ls\phi s\theta s\psi - \tau_8)\, c\phi s\psi \\ +l(y + lc\phi c\psi + ls\phi s\theta s\psi - \tau_8)\, s\phi s\theta c\psi \end{pmatrix} + \frac{\xi_3 G}{S_3^2}\psi,$$

$$g_4 = 1 + \frac{\gamma_4 G}{D_4^2}, \quad g_5 = 1 + \frac{\gamma_5 G}{D_5^2}, \quad g_6 = 1 + \frac{\gamma_6 G}{D_6^2}.$$

Let

$$f_1\dot{x} + f_4 v\dot{v} = -\delta_1 v^2, \quad (23)$$

$$f_2\dot{y} + f_5 w\dot{w} = -\delta_2 w^2, \quad (24)$$

$$f_3\dot{z} + f_6 u\dot{u} = -\delta_3 u^2, \quad (25)$$

$$g_1\dot{\phi} + g_4 q\dot{q} = -\delta_4 q^2, \quad (26)$$

$$g_2\dot{\theta} + g_5 p\dot{p} = -\delta_5 p^2, \quad (27)$$

$$g_3\dot{\psi} + g_6 r\dot{r} = -\delta_6 r^2, \quad (28)$$

where $\delta_i > 0$, and $i = 1, \ldots, 6$ are called the *convergence parameters*. Substituting (23–28) into (22), we have

$$\dot{L}_{(6)}(\mathbf{x}) = -\delta_1 v^2 - \delta_2 w^2 - \delta_3 u^2 - \delta_4 q^2 - \delta_5 p^2 - \delta_6 r^2 \leq 0, \quad (29)$$

provided we define the nonlinear control inputs as,

$$\left.\begin{aligned} U_{1x} &:= \frac{-m\,(f_1+\delta_1 v)+f_4\kappa_1 v}{f_4\ (\cos\phi\sin\theta\cos\psi+\sin\phi\sin\psi)},\\ U_{1y} &:= \frac{-m\,(f_2+\delta_2 w)+f_5\,\kappa_2 w}{f_5\,(\cos\phi\sin\theta\sin\psi\ -\sin\phi\cos\psi)},\\ U_{1z} &:= \frac{-m\,(f_3+\delta_3 u-f_6\ g)+f_6\kappa_3 u}{f_6\,(\cos\theta\cos\phi)},\\ U_2 &:= \frac{-I_x\,(g_1+\delta_4 q)+g_4 l\kappa_4 q}{g_4\ l},\\ U_3 &:= \frac{-I_y\,(g_2+\delta_5 p)+g_5 l\kappa_5 p}{g_5\ l},\\ U_4 &:= \frac{-I_z\,(g_3\ +\delta_6 r)+g_6\kappa_6 r}{g_6}. \end{aligned}\right\} \tag{30}$$

V. STABILITY ANALYSIS

In this section, we shall show that every bounded solution $\mathbf{x}(t)$ of (6), as $t\to+\infty$, converges to the point

$$\mathbf{x}_e := (\tau_1,\tau_2,\tau_3,0,0,0,\phi_f,\theta_f,\psi_f,0,0,0)\in\mathbb{D}(L),$$

where ϕ_f, θ_f and ψ_f are the final orientations. Ideally, the final pitch and roll angles (i.e., ϕ_f and θ_f) should be zero at the target (τ_1,τ_2,τ_3), where $(v,w,u)=(0,0,0)$ and $(p,q,r)=(0,0,0)$.

Now, on substituting the controllers (30) into (6), we have

$$\left.\begin{aligned} &\dot{x}=v,\ \dot{y}=w,\ \dot{z}=u,\\ &\dot{v}=\frac{f_1+\delta_1 v}{f_4},\ \dot{w}=\frac{f_2+\delta_2 w}{f_5},\ \dot{u}=\frac{f_3+\delta_3 u}{f_6},\\ &\dot{\phi}=q,\ \dot{\theta}=p,\ \dot{\psi}=r,\\ &\dot{q}=\frac{g_1+\delta_4 q}{g_4},\ \dot{p}=\frac{g_2+\delta_5 p}{g_5},\ \dot{r}=\frac{g_3+\delta_6 r}{g_6}. \end{aligned}\right\} \tag{31}$$

Recalling that

$$\begin{aligned}\mathbf{x}&=(x_1,\ldots,x_{12})\\ &=(x,y,z,\phi,\theta,\psi,v,w,u,q,p,r)\in\mathbb{R}^{12},\end{aligned}$$

we can see that an equilibrium point of system (31) is indeed $\mathbf{x}_e$. Then (31) can be written simply as the initial-value problem

$$\dot{\mathbf{x}}=\mathbf{H}(\mathbf{x}),\quad \mathbf{x}_0:=\mathbf{x}(0). \tag{32}$$

where

$$\begin{aligned}\mathbf{H}(\mathbf{x})&:=(h_1(\mathbf{x}),\ldots,h_{12}(\mathbf{x}))\\ &:=\left(\dot{x},\dot{y},\dot{z},\dot{\phi},\dot{\theta},\dot{\psi},\dot{v},\dot{w},\dot{u},\dot{q},\dot{p},\dot{r}\right)\end{aligned}$$

We shall use the following result by Yoshizawa [38], taken from Burton [39] (page 161) to establish the convergence of the solution $\mathbf{x}$ of (32) to $\mathbf{x}_e$ in $\mathbb{D}(L)$.

Consider a system of ODEs

$$X'(t)=\mathcal{H}(t,X(t)),\quad \mathcal{H}(t,0)=0, \tag{33}$$

in which $\mathcal{H}:[0,\infty)\times\mathcal{D}\to\mathbb{R}^n$ is continuous and $\mathcal{D}$ is an open set in $\mathbb{R}^n$ with 0 in $\mathcal{D}$.

For our purpose a scalar function $\mathcal{W}:\mathbb{R}^n\to[0,\infty)$ is *positive definite with respect to a set* $\mathcal{A}$ if $\mathcal{W}(X)=0$ for $X\in\mathcal{A}$ and for each $\varepsilon>0$ and each compact set $\mathcal{Q}$ in $\mathbb{R}^n$ there exists $\delta=\delta(\mathcal{Q},\varepsilon)$ such that $\mathcal{W}(\mathbf{x})\geq\delta$ for $X\in\mathcal{Q}\cap\mathcal{U}(\mathcal{A},\varepsilon)^c$ where $\mathcal{U}(\mathcal{A},\varepsilon)$ is the ε-neighbourhood of $\mathcal{A}$.

Theorem 1 (Yoshizawa (1963)): Let $\mathcal{D}=\mathbb{R}^n$ and let $\mathcal{H}(t,X)$ be bounded for X bounded. Also suppose that all solutions of (33) are bounded. If there is a continuous function $\mathcal{V}:[0,\infty)\times\mathbb{R}^n\to[0,\infty)$ that is locally Lipschitz in X, if there is a continuous function $\mathcal{W}:\mathbb{R}^n\to[0,\infty)$ that is positive definite with respect to a closed set Ω, and if $\mathcal{V}'_{33}(t,X)\leqslant-\mathcal{W}(X)$, then every solution of (33) approaches Ω as $t\to\infty$.

Remark 1: Note that in Theorem 1, the requirement that all solutions should be bounded can be dropped and the conclusion changed to read that all bounded solutions approach Ω.

We first establish the boundedness of $\mathbf{H}(\mathbf{x})$ for $\mathbf{x}$ bounded using a recently published approach in Vanualailai [40].

Lemma 1: In system (32), the function $\mathbf{H}\in C[\mathbb{D}(L),\mathbb{R}^{12}]$ is bounded if $\mathbf{x}\in\mathbb{D}(L)$ is bounded.

Proof: In the functions f_i and g_i, $i=1,2,3,4$, we see that the functions that appear in the denominator are S_s, $s=1,2,3$, and D_d, $d=1,\cdots,6$. Hence, we can easily conclude that $\mathbf{H}\in C[\mathbb{D}(L),\mathbb{R}^{12}]$, which implies that at least on some time interval $[t_0,\alpha]$, $\alpha>0$, the solution $\mathbf{x}(t)$ of system (32) exists and is in $\mathbb{D}(L)$. Indeed, these functions will also appear in the denominator in higher-order partial derivatives of f_i and g_i, $i=1,2,3,4$, with each derivative continuous on $\mathbb{D}(L)$. That is, since $\mathbf{H}\in C^1[D(L),\mathbb{R}^{12}]$, we have that $\mathbf{H}$ is locally Lipschitz on $\mathbb{D}(L)$ on the time interval $[t_0,\alpha]$. We shall next show that $\mathbf{x}(t)$ exists and is unique for all time $t\geq t_0\geq0$ in $\mathbb{D}(L)$, so that we can conclude that $\mathbb{H}$ is globally continuous on $\mathbb{D}(L)$.

We begin by observing that since the time-derivative of L along the solution of (32) is non-positive, we have

$$L(\mathbf{x}(t))\leq L_0:=L(\mathbf{x}_0),\quad t\in[t_0,\alpha].$$

Thus, given the form of L in (21), we easily see that for each $s=1,2,3$, and each $d=1,\ldots,6$,

$$\frac{\xi_s G(\mathbf{x}(t))}{S_s(\mathbf{x}(t))}\leq L_0 \text{ and } \frac{\gamma_d G(\mathbf{x}(t))}{D_d(\mathbf{x}(t))}\leq L_0,\quad t\in[t_0,\alpha].$$

Given the form of G, and letting $M_0:=L_0/\epsilon^2$, we have therefore

$$\frac{1}{S_s(\mathbf{x}(t))}\leq\frac{\xi_s G(\mathbf{x}(t))}{\epsilon^2 S_s(\mathbf{x}(t))}\leq M_0,\quad t\in[t_0,\alpha], \tag{34}$$

and

$$\frac{1}{D_d(\mathbf{x}(t))}\leq\frac{\gamma_d G(\mathbf{x}(t))}{\epsilon^2 D_d(\mathbf{x}(t))}\leq M_0,\quad t\in[t_0,\alpha]. \tag{35}$$

Thus, if $\xi_0:=\max\{\xi_s,s=1,2,3\}$, and $\gamma_0:=\max\{\gamma_d,d=1,\ldots,6\}$, then, in view of (34) and (35), we have, with $K_0:=1+3\xi_0 M_0+6\gamma_0 M_0$, the inequalities,

$$\begin{aligned}|f_1|&\leq\left(1+\xi_0\sum_{s=1}^{3}\frac{1}{S_s}+\gamma_0\sum_{d=1}^{6}\frac{1}{D_d}\right)|x-\tau_1|\\ &\quad+2|x-\tau_1|+4\,l\\ &\leq K_0\,|x-\tau_1|+2|x-\tau_1|+4\,l,\end{aligned}$$

TABLE 1. Parameters of the quadrotor UAV pertaining to Scenario 1.

Description	Value	Units
Initial state of the quadrotor		
Position	$(x, y, z) = (0, 0, 0)$	
Angles	$\phi = \theta = \psi = 0$	rad
Translational velocities	$v = w = u = 0.5$	m/s
Rotational velocities	$q = p = r = 0$	rad/s
Parameters		
Error in $G(\mathbf{x})$	$\epsilon = 10^{-12}$	
Mass	$m = 2$	kg
Length	$l = 0.2$	m
Gravitational acceleration	$g = 9.8$	m/s^2
Moments of inertia	$I_x = I_y = 4.856 \times 10^{-3}$, and $I_z = 4.856 \times 10^{-2}$	kgm^2
Drag coefficient	$\kappa_i = 0.01$, for $i = 1, \ldots, 3$ and $\kappa_i = 0.012$ for $i = 1, \ldots, 3$	Ns/m
Target position	$(\tau_1, \tau_2, \tau_3) = (0, 0, 85)$	
Maximum translational velocities	$v_{max} = w_{max} = u_{max} = 1$	m/s
Maximum rotational velocities	$q_{max} = p_{max} = r_{max} = 1$	rad/s
Constraints for the quadrotor		
Dynamic constraints on the angles	$\xi_s = 50$ for $s = 1, \ldots, 3$	
Dynamic constraints on the velocities	$\gamma_1 = 0.5$, $\gamma_2 = 0.5$, $\gamma_3 = 1 \times 10^{-6}$, $\gamma_4 = \gamma_5 = \gamma_6 = 50$	
Convergence	$\delta_1 = 0.01$, $\delta_2 = 0.05$, $\delta_3 = 1000$, $\delta_4 = 2$, $\delta_5 = 1$ and $\delta_6 = 5$	

$$
\begin{aligned}
|f_2| &\le \left(1 + \xi_0 \sum_{s=1}^{3} \frac{1}{S_s} + \gamma_0 \sum_{d=1}^{6} \frac{1}{D_d}\right) |y - \tau_2| \\
&\quad + 2|y - \tau_2| + 4\,l \\
&\le K_0\,|y - \tau_2| + 2|y - \tau_2| + 4\,l,
\end{aligned}
$$

$$
\begin{aligned}
|f_3| &\le \left(1 + \xi_0 \sum_{s=1}^{3} \frac{1}{S_s} + \gamma_0 \sum_{d=1}^{6} \frac{1}{D_d}\right) |z - \tau_3| \\
&\quad + 2|z - \tau_3| + 2l \\
&\le K_0\,|z - \tau_3| + 2|z - \tau_3| + 2l.
\end{aligned}
$$

Now, in real-life situations, the half-length l of the quadrotor negligibly small compared to the distance between the quadrotor and its target (τ_1, τ_2, τ_3), with $l \ll |x - \tau_1|, |y - \tau_2|, |z - \tau_3|$. Then, since $1/f_i \le 1$, $i = 4, 5, 6$, we have

$$
\begin{aligned}
|\dot{v}| &\le |f_1| + \gamma_1|v| \le (K_0 + 6)|x - \tau_1| + \gamma_1|v|, \\
|\dot{w}| &\le |f_2| + \gamma_2|w| \le (K_0 + 6)|y - \tau_2| + \gamma_2|w|, \\
|\dot{u}| &\le |f_3| + \gamma_3|u| \le (K_0 + 6)|z - \tau_3| + \gamma_3|u|.
\end{aligned}
$$

Noting that $V_1(\mathbf{x}(t)) = G(\mathbf{x}(t)) \le L_0$ for $t \in [t_0, \alpha]$, we have

$$
|g_1| \le N_0|\phi|, \quad |g_2| \le N_0|\theta| \quad \text{and} \quad |g_3| \le N_0|\psi|,
$$

where $N_0 := \xi_0\, L_0 M_0^2$. Since $1/g_i \le 1$, $i = 4, 5, 6$, we have

$$
\begin{aligned}
|\dot{q}| &\le |g_1| + \delta_4|q| \le N_0|\phi| + \delta_4|q|, \\
|\dot{p}| &\le |g_2| + \delta_5|q| \le N_0|\theta| + \delta_5|p|, \\
|\dot{r}| &\le |g_3| + \delta_6|r| \le N_0|\psi| + \delta_6|r|.
\end{aligned}
$$

Hence,

$$
\begin{aligned}
\|\mathbf{H}\| &\le (K_0 + 6)(|x - \tau_1| + |y - \tau_2| + |z - \tau_3|) \\
&\quad + (1 + \delta_1)|v| + (1 + \delta_2)|w| + (1 + \delta_3)|u| \\
&\quad + N_0(|\phi| + |\theta| + |\psi|) \\
&\quad + (1 + \delta_4)|q| + (1 + \delta_5)|p| + (1 + \delta_6)|r|,
\end{aligned}
$$

so that if $K := \max\{(1 + \delta_1), (1 + \delta_2), (1 + \delta_3), (1 + \delta_4), (1 + \delta_5), (1 + \delta_6), K_0 + 6, N_0\}$, then

$$
\begin{aligned}
\|\mathbf{H}\| \le K\,(&|x - \tau_1| + |y - \tau_2| + |z - \tau_3| \\
&+ |v| + |w| + |\phi| + |\theta| + |\psi||u| \\
&+ |q| + |p| + |r|)\,.
\end{aligned}
$$

Accordingly, for some constant $M > 0$ independent of α, we have

$$
\|\mathbf{H}(\mathbf{x})\| \le M\|\mathbf{x} - \mathbf{x}_e\|, \tag{36}
$$

where $\mathbf{x}_e = (\tau_1, \tau_2, \tau_3, 0, \ldots, 0) \in \mathbb{R}^{12}$. Let $\mathbf{u} = \mathbf{x} - \mathbf{x}_e$. Then,

$$
\begin{aligned}
\frac{1}{2}\frac{d}{dt}\|\mathbf{u}(t)\|^2 &= \langle \mathbf{u}(t), \dot{\mathbf{u}}(t)\rangle = \langle \mathbf{u}(t), \mathbf{G}_p(\mathbf{x}(t))\rangle \\
&\le \|\mathbf{u}(t)\|\,\|\mathbf{G}_p(\mathbf{x}(t))\| \\
&\le M\|\mathbf{u}(t)\|^2.
\end{aligned} \tag{37}
$$

Let $\zeta(t) := \|\mathbf{u}(t)\|^2$. Then we have the differential inequality,

$$
\frac{1}{2}\frac{d}{dt}\zeta(t) \le M\zeta(t), \quad \zeta(t_0) = \|\mathbf{u}(t_0)\|^2. \tag{38}
$$

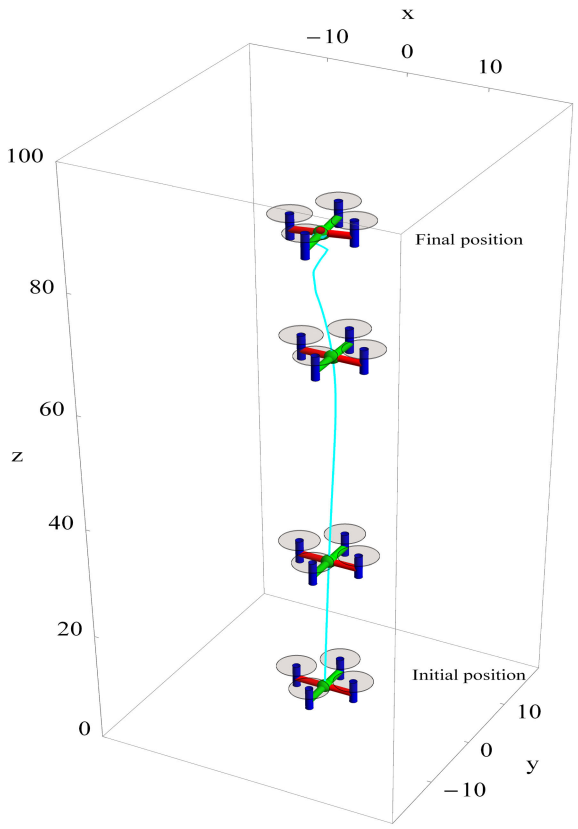

FIGURE 5. The quadrotor motion at $t = 0, 10, 36, 300$ units of time in Scenario 1. The quadrotor maintains a smooth trajectory (shown in cyan) en route to its target and starts hovering from $t_\tau = 90$ unit of time.

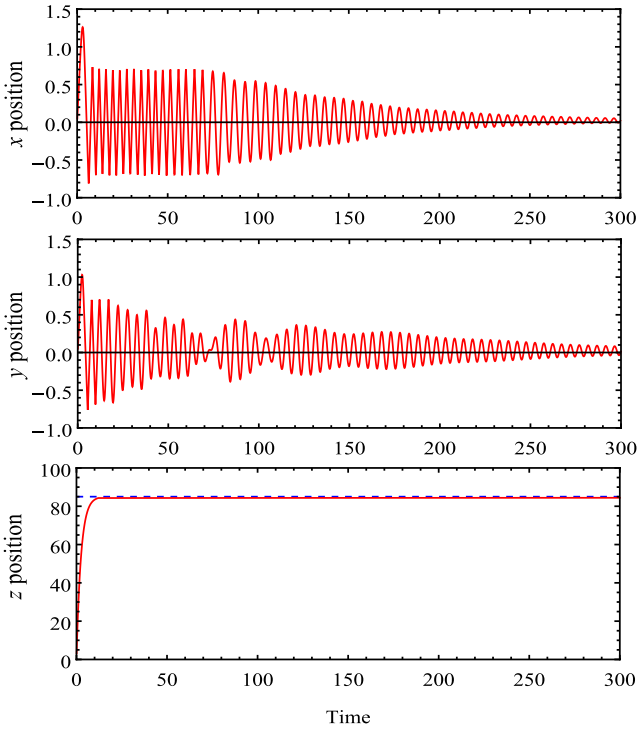

FIGURE 6. The responses for the displacements pertaining to Scenario 1. The *x* and *y* positions oscillate about and converge to zero as the controllers converge to zero as time goes to infinity. The blue line in the *z* position is indicative of the quadrotor reaching its target and hovering.

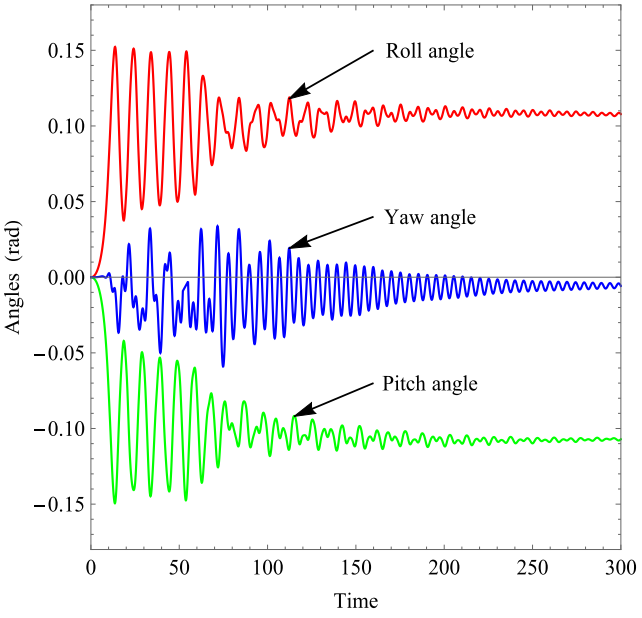

FIGURE 7. The responses of attitudes by the proposed controllers corresponding to Scenario 1. The roll, pitch and yaw angle motions are shown in red, green and blue, respectively.

Comparing (37) and (38), it is easy to see that $\|\mathbf{u}(t)\|^2 \leq \|\mathbf{u}(t_0)\|^2 e^{2K(t-t_0)}$ for $t \in [t_0, s]$. This implies the existence of the solution $\mathbf{x}(t)$ of system (32) on $[t_0, \alpha + \rho]$, $\rho > 0$ being independent of $\alpha > 0$. Hence, we can conclude that $\mathbf{H}(\mathbf{x})$ is globally Lipschitz continuous on $\mathbb{D}(L)$.

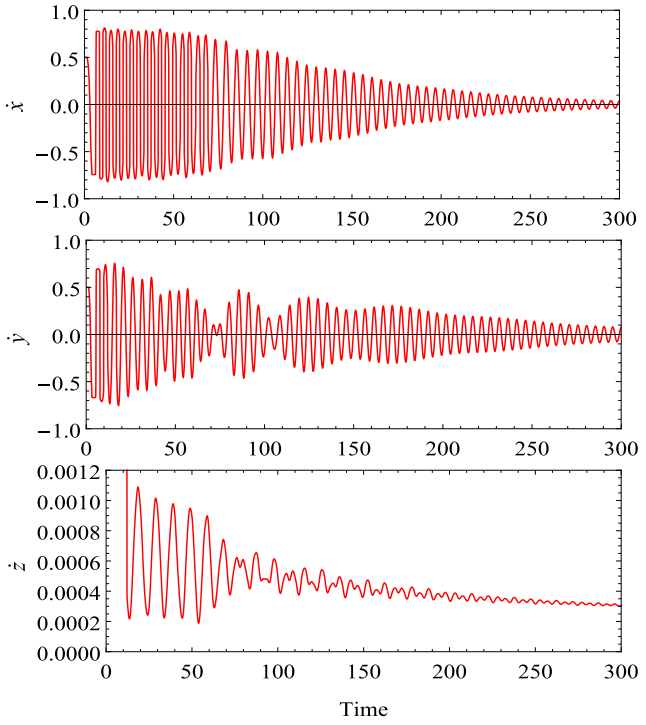

FIGURE 8. The responses of the translational velocities in Scenario 1. The velocities are approaching zero, enabling the quadrotor to hover.

In addition, equation (36) shows that $\mathbf{H}(\mathbf{x})$ is bounded if $\mathbf{x} \in \mathbb{D}(L)$ is bounded.

We have thus proven Lemma 1.

Q.E.D.

We now come to the main theorem on the convergence of solutions.

Theorem 2: Every bounded solution $\mathbf{x}(t)$ in $\mathbb{D}(L)$ of (32) converges to

$$\Omega := \{\mathbf{x} \in \mathbb{D}(L) : v = w = u = p = q = r = 0\}$$

as $t \to \infty$.

Proof: Given the Lyapunov-like function L in (20) and its derivative $\dot{L}$ in (29), we see that $L \in C^1[\mathbb{D}(L), \mathbb{R}_+]$, $\mathbb{R}_+ := [0, \infty)$. Hence L is locally Lipschtiz in $\mathbf{x} \in \mathbb{D}(L)$. Now, let $\mathcal{W}(\mathbf{x}) := -\dot{L}(\mathbf{x})$. It is clear that it is positive definite with respect to Ω. Thus, given Lemma 1, the conclusion of Theroem 2 follows from Yoshizawa's Theorem (1).

Q.E.D.

Remark 2: We note that $v = w = u = p = q = r = 0$ at $\mathbf{x}_e$, and therefore at the target (τ_1, τ_2, τ_3).

VI. SIMULATIONS

In order to exhibit the effectiveness of the proposed novel controllers, computer simulations using virtual scenarios are carried out. The scenarios involve a quadrotor that navigates to a final configuration while the dynamic constraints associated with the dynamic model are satisfied.

We note here that in the previous Lyapunov-based methods, the major difficulty was obtaining hovering maneuvers

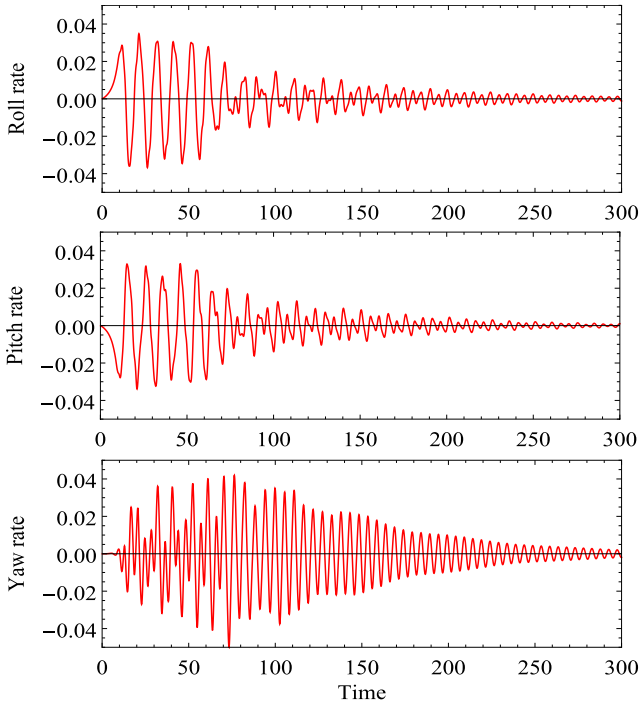

FIGURE 9. The responses of the rotational velocities in Scenario 1.

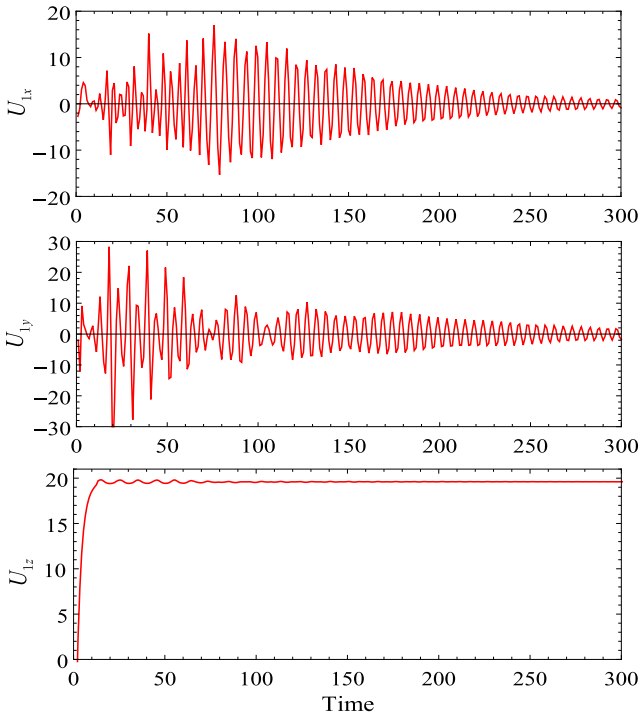

FIGURE 10. The constituents of controller $U_1 = \sqrt{U_{1x}^2 + U_{1y}^2 + U_{1z}^2}$ in Scenario 1.

within a neighborhood of the target. In the simulation of these methods, the solutions diverge in a neighborhood of the target, and therefore there was a need to stop the simulation. In these methods, the main purpose is to show the effectiveness of the controllers to take the quadrotor to its target but

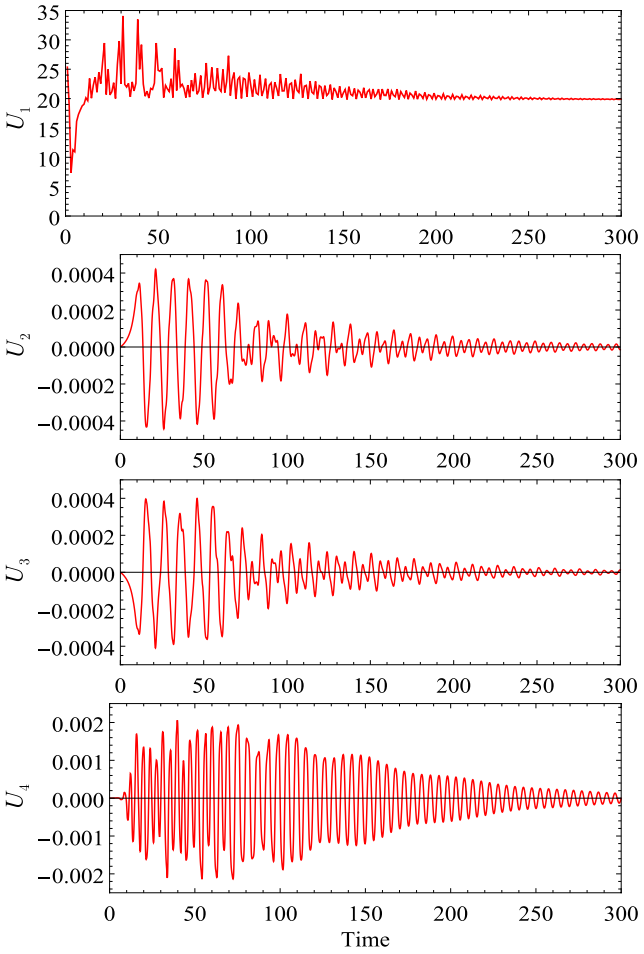

FIGURE 11. The responses of the control forces and torques by the proposed controllers in Scenario 1.

not hovering [3], [10]. Our methodology solves this problem completely where our solutions converge to the target and remains there.

A. SCENARIO 1 - VERTICAL TAKE-OFF AND HOVERING

To show the effectiveness, robustness and the simplicity of the proposed control laws, the first scenario exhibits a vertical take-off maneuver for the quadrotor from an initial position to its target configuration. The trajectory of the quadrotor aircraft en route to its target is very smooth and the quadrotor motion is observed to be hovering about its target. This is a novel contribution of this paper, that is, via the new controllers, the quadrotor hovers over the target for $t > t_\tau$, where t_τ is the time it takes the quadrotor to reach its target. Table 1 provides all the values of the initial conditions, constraints and different parameters utilised in the simulation. The quadrotor flight motion is shown in Fig. 5. Fig. 6 shows the displacement of the quadrotor at any time $t > 0$. The control scheme ensures that the quadrotor UAV maintains attitude angles to allow it to hover over the target configuration. Fig. 7 shows the attitude angles corresponding to this scenario. The angles aid in attaining the hovering motion of the quadrotor. Fig. 8 and Fig. 9 show the translational and

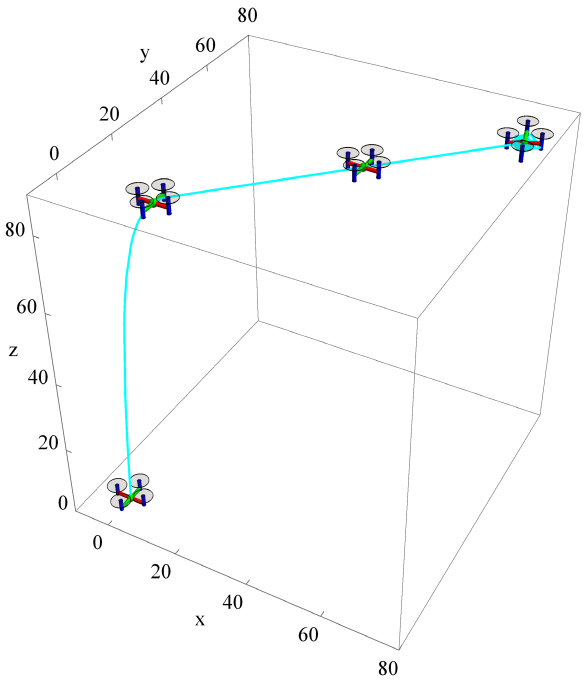

FIGURE 12. The quadrotor motion at $t = 0, 10, 45, 250$ units of time in Scenario 2. The quadrotor maintains a smooth trajectory (shown in cyan) en route to its target, reaching a vicinity of its target $t_\tau = 70$ unit of time and continuously hovers about its target configuration.

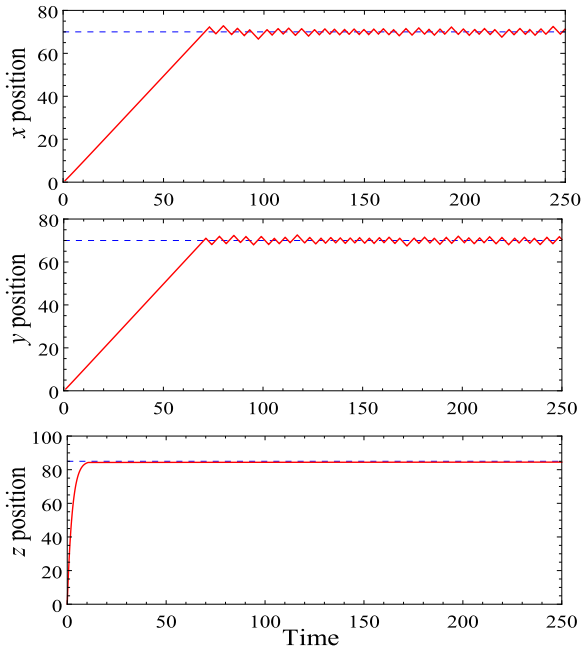

FIGURE 13. The responses for the displacements pertaining to scenario 2. The x and y position fluctuations are a result of the control scheme trying to attain zero. The blue line in the x, y and z position is indicative of the quadrotor reaching its target position and hovering.

rotational velocities, respectively of the quadrotor. Fig. 10 shows the constituents of the controller U_1. Fig 11 illustrates the control inputs corresponding to the parameters utilised in the scenario.

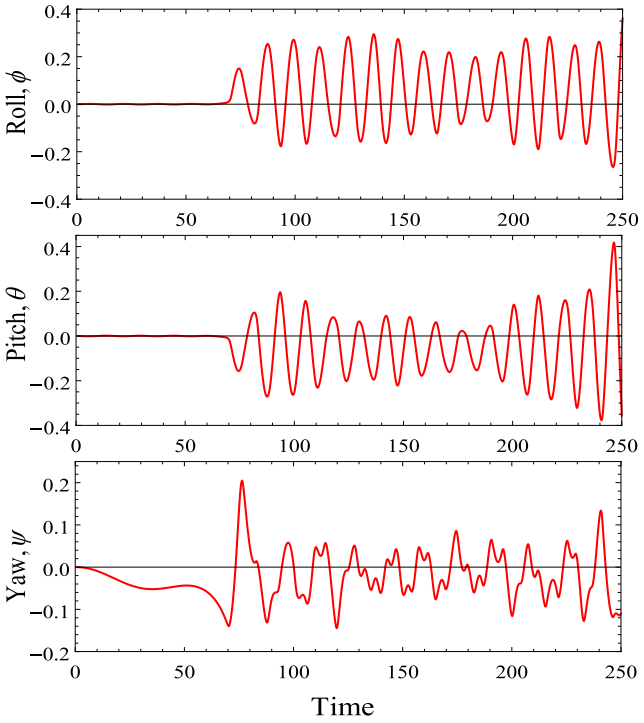

FIGURE 14. The responses of attitudes by the proposed controllers corresponding to Scenario 2. The roll, pitch and yaw angle motions are shown in red, green and blue, respectively.

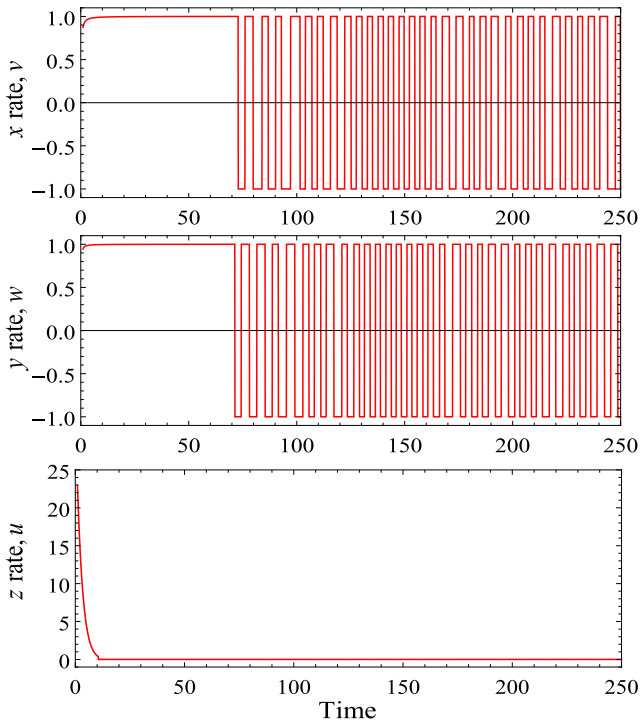

FIGURE 15. The responses of the translational velocities in Scenario 2. The velocities are approaching its maximum to allow the quadrotor to hover about the target configuration.

We note here that a similar work has been done by Bouabdallah in 2004 [10], who was able to show only the vertical take-off maneuvers. In this simulation, we are able to show

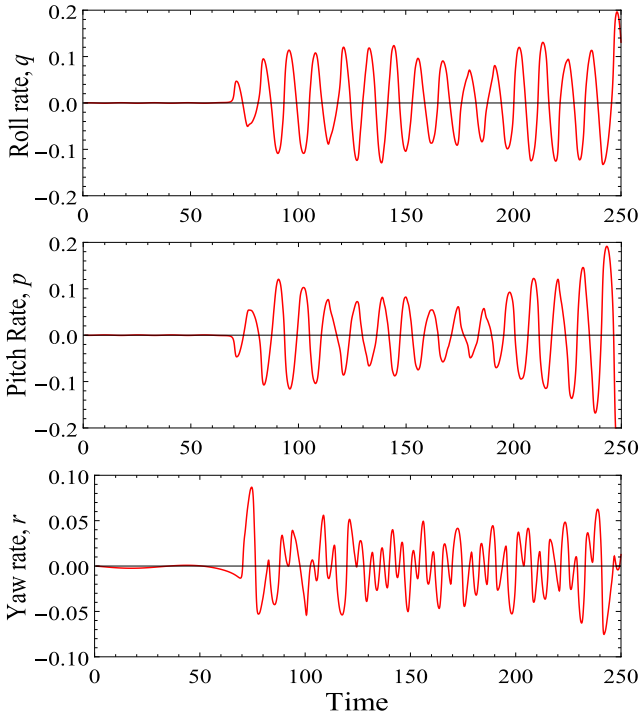

FIGURE 16. The responses of the rotational velocities in Scenario 2.

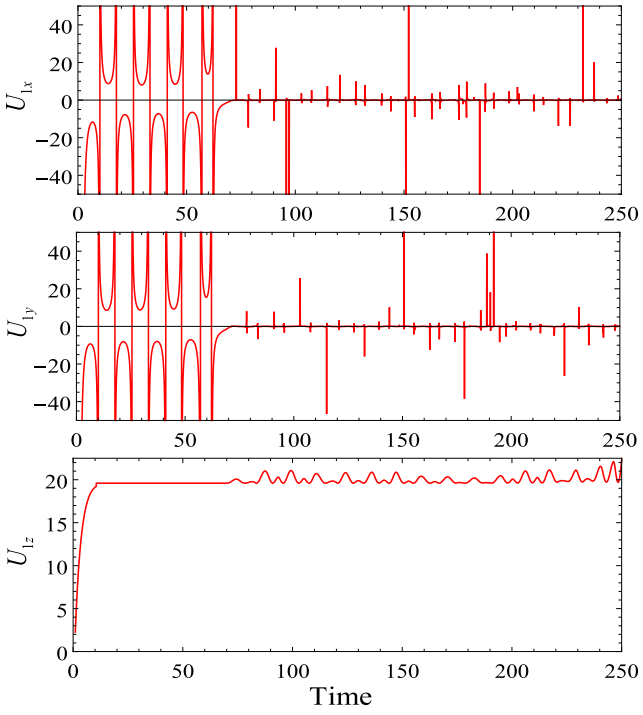

FIGURE 17. The constituents of controller U_1 in Scenario 2.

not only the vertical take-off maneuvers but also that the quadrotor has near-to-horizontal orientation during its flight and hovering maneuvers about the neighborhood of the target.

B. SCENARIO 2

This scenario illustrates the hovering maneuvers about the target configuration. The quadrotor starts from its initial position

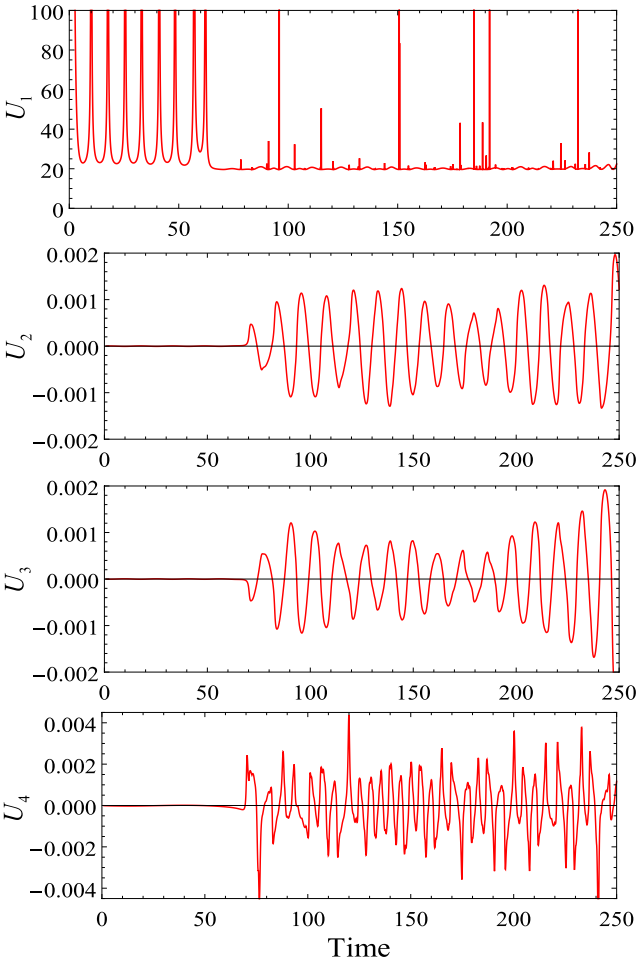

FIGURE 18. The responses of the control forces and torques by the proposed controllers in Scenario 2.

TABLE 2. Parameters of the quadrotor UAV pertaining to Scenario 2.

Parameters		
Drag coefficient	$\kappa_i = 0.01$, for $i = 1, \ldots, 6$	Ns/m
Target position	$(\tau_1, \tau_2, \tau_3) = (50, 90, 85)$	
Constraints for the quadrotor		
Dynamic constraints on the angles	$\xi_s = 100$ for $s = 1, \ldots, 3$	
Dynamic constraints on the velocities	$\gamma_1 = 1$, $\gamma_2 = 2$, $\gamma_3 = 0.5$, $\gamma_4 = \gamma_5 = \gamma_6 = 100$	
Convergence	$\delta_1 = 0.1$, $\delta_2 = 0.2$, $\delta_3 = 0.05$, $\delta_4 = 2$, $\delta_5 = 1$ and $\delta_6 = 0.5$	

and maintains a near-to-horizontal orientation en route to its target. The quadrotor is observed to reach its target at time $t_\tau = 70$ unit of time and is observed to hover about the vicinity of the target by rolling, pitching and yawing. At each time, the quadrotor stabilises itself such that it does not pitch or roll too much and maintains its near-to-horizontal orientation. This feature is essential for the delivery of fragile packages safely and precisely to the target location. Table 2 provides all the values of the initial conditions, constraints and different parameters utilised in the simulation, if the values therein are different from those used in the previous scenario.

The quadrotor flight motion for Scenario 2 is shown in Fig. 12. Fig. 13 shows the altitude of the quadrotor. The control scheme has to maintain attitude angles to allow the quadrotor to hover about a certain vicinity of the target configuration. Fig. 14 shows the attitude angles which aid in attaining the hovering motion of the quadrotor. Fig. 15 and Fig. 16 show the translational and rotational velocities of the quadrotor, respectively. Fig. 17 shows the constituents of the controller U_1. Fig 18 illustrates the control inputs corresponding to the parameters utilised in Scenario 2.

VII. CONCLUSION

The design and simulation of autonomous controllers of UAVs, though complex and computer intensive, is an interesting problem. In this paper, a set of nonlinear control laws for a quadrotor were derived using a Lyapunov-based control scheme (LbCS). The continuous time-invariant acceleration control laws govern the motion, namely the attitude, altitude and position, of the quadrotor.

To the author's knowledge, this is the first time in literature whereby the quadrotor is successfully controlled via the LbCS to ensure the hovering of the quadrotor within a vicinity of the target configuration. Another novel feature of the new controllers is that they allow a near-to-horizontal orientation of the quadrotor at each point in time whilst navigating from some initial configuration to a final configuration. This is important if the payload is sensitive to unsteady motion. Moreover, the control laws guaranteed the stability of the dynamic model.

This paper is a theoretical exposition into the application of the Artificial Potential Fields (APF) method for the control of quadrotors. We restrict ourselves to showing the effectiveness of the proposed control laws using computer-based simulations. Future work in this area includes applying the LbCS motion planner to address the motion planning and control problem of a flock of quadrotors performing hovering maneuvers in the presence of obstacles.

ACKNOWLEDGMENT

The authors would like to acknowledge the anonymous reviewers for their comments which led to the enhancement of the quality and presentation of this article.

REFERENCES

[1] V. Kumar and N. Michael, "Opportunities and challenges with autonomous micro aerial vehicles," *Int. J. Robot. Res.*, vol. 31, no. 11, pp. 1279–1291, 2012.

[2] H. Rios, R. Falcon, O. A. Gonzalez, and A. Dzul, "Continuous sliding-mode control strategies for quadrotor robust tracking: Real-time application," *IEEE Trans. Ind. Electron.*, vol. 66, no. 2, pp. 1264–1272, Feb. 2019.

[3] S. Bouabdallah, P. Murrieri, and R. Siegwart, "Design and control of an indoor micro quadrotor," in *Proc. IEEE Int. Conf. Robot. Autom. (ICRA)*, vol. 5, Apr. 2004, pp. 4393–4398.

[4] M. Mardan, M. Esfandiari, and N. Sepehri, "Attitude and position controller design and implementation for a quadrotor," *Int. J. Adv. Robotic Syst.*, vol. 14, no. 3, May 2017, Art. no. 172988141770924.

[5] Z. Liu, X. Liu, J. Chen, and C. Fang, "Altitude control for variable load quadrotor via learning rate based robust sliding mode controller," *IEEE Access*, vol. 7, pp. 9736–9744, 2019.

[6] X. Huo, M. Huo, and H. R. Karimi, "Attitude stabilization control of a quadrotor UAV by using backstepping approach," *Math. Problems Eng.*, vol. 2014, Feb. 2014, Art. no. 749803.

[7] A. Poultney, C. Kennedy, G. Clayton, and H. Ashrafiuon, "Robust tracking control of quadrotors based on differential flatness: Simulations and experiments," *IEEE/ASME Trans. Mechatronics*, vol. 23, no. 3, pp. 1126–1137, Jun. 2018.

[8] D. Falanga, K. Kleber, S. Mintchev, D. Floreano, and D. Scaramuzza, "The foldable drone: A morphing quadrotor that can squeeze and fly," *IEEE Robot. Autom. Lett.*, vol. 4, no. 2, pp. 209–216, Apr. 2019.

[9] A. Das, F. Lewis, and K. Subbarao, "Backstepping approach for controlling a quadrotor using Lagrange form dynamics," *J. Intell. Robot. Syst.*, vol. 56, nos. 1–2, pp. 127–151, Sep. 2009.

[10] S. Bouabdallah, A. Noth, and R. Siegwart, "PID vs LQ control techniques applied to an indoor micro quadrotor," in *Proc. IEEE/RSJ Int. Conf. Intell. Robots Syst. (IROS)*, vol. 3, Sep. 2004, pp. 2451–2456.

[11] M. Nguyen Duc, T. N. Trong, and Y. S. Xuan, "The quadrotor MAV system using PID control," in *Proc. IEEE Int. Conf. Mechatronics Autom. (ICMA)*, Aug. 2015, pp. 506–510.

[12] Y. Sun, N. Xian, and H. Duan, "Linear-quadratic regulator controller design for quadrotor based on pigeon-inspired optimization," *Aircr. Eng. Aerosp. Technol.*, vol. 88, no. 6, pp. 761–770, Oct. 2016.

[13] R. Xu and U. Ozguner, "Sliding mode control of a quadrotor helicopter," in *Proc. 45th IEEE Conf. Decis. Control*, San Diego, CA, USA, Dec. 2006, pp. 4957–4962.

[14] F. Muñoz, I. González-Hernández, S. Salazar, E. S. Espinoza, and R. Lozano, "Second order sliding mode controllers for altitude control of a quadrotor UAS: Real-time implementation in outdoor environments," *Neurocomputing*, vol. 233, pp. 61–71, Apr. 2015.

[15] W. Jasim and D. Gu, "H_∞ for quadrotor attitude stabilization," in *Proc. UKACC Int. Conf. Control (CONTROL)*, Jul. 2014, pp. 19–24.

[16] E. Kayacan and R. Maslim, "Type-2 fuzzy logic trajectory tracking control of quadrotor VTOL aircraft with elliptic membership functions," *IEEE/ASME Trans. Mechatronics*, vol. 22, no. 1, pp. 339–348, Feb. 2017.

[17] K. E. Wenzel, P. Rosset, and A. Zell, "Low-cost visual tracking of a landing place and hovering flight control with a microcontroller," *J. Intell. Robot. Syst.*, vol. 57, p. 297, Aug. 2009.

[18] H. Chen and N. Sun, "Nonlinear control of underactuated systems subject to both actuated and unactuated state constraints with experimental verification," *IEEE Trans. Ind. Electron.*, to be published.

[19] J. Raj, K. Raghuwaiya, S. Singh, B. Sharma, and J. Vanualailai, "Swarming intelligence of 1-trailer systems," in *Advanced Computer and Communication Engineering Technology*, H. A. Sulaiman, M. A. Othman, M. F. I. Othman, Y. A. Rahim, and N. C. Pee, Eds. Cham, Switzerland: Springer, 2016, pp. 251–264.

[20] K. Raghuwaiya, B. Sharma, and J. Vanualailai, "Leader-follower based locally rigid formation control," *J. Adv. Transp.*, vol. 2018, pp. 1–14, Feb. 2018.

[21] B. N. Sharma, J. Raj, and J. Vanualailai, "Navigation of carlike robots in an extended dynamic environment with swarm avoidance," *Int. J. Robust Nonlinear Control*, vol. 28, no. 2, pp. 678–698, Jan. 2018.

[22] J. Raj, K. Raghuwaiya, J. Vanualailai, and B. Sharma, "Navigation of car-like robots in three-dimensional space," in *Proc. 5th Asia–Pacific World Congr. Comput. Sci. Eng. (APWC CSE)*, Dec. 2018, pp. 271–275.

[23] O. Khatib, "Real time obstacle avoidance for manipulators and mobile robots," *Int. J. Robot. Res.*, vol. 7, no. 1, pp. 90–98, 1986.

[24] J.-P. Laumond, P. E. Jacobs, M. Taix, and R. M. Murray, "A motion planner for nonholonomic mobile robots," *IEEE Trans. Robot. Autom.*, vol. 10, no. 5, pp. 577–593, Oct. 1994.

[25] B. J. Bialy, J. Klotz, K. Brink, and W. E. Dixon, "Lyapunov-based robust adaptive control of a quadrotor UAV in the presence of modeling uncertainties," in *Proc. Amer. Control Conf.*, Jun. 2013, pp. 13–18.

[26] A. Yesildirek and B. Imran, "Nonlinear control of quadrotor using multi Lyapunov functions," in *Proc. Amer. Control Conf.*, Jun. 2014, pp. 3844–3849.

[27] A. Safaei and M. N. Mahyuddin, "Lyapunov-based nonlinear controller for quadrotor position and attitude tracking with GA optimization," in *Proc. IEEE Ind. Electron. Appl. Conf. (IEACon)*, Nov. 2016, pp. 342–347.

[28] N. Liu, X. Shao, and W. Yang, "Integral barrier Lyapunov function based saturated dynamic surface control for vision-based quadrotors via backstepping," *IEEE Access*, vol. 6, pp. 63292–63304, 2018.

[29] H. Chen, B. Xuan, P. Yang, and H. Chen, "A new overhead crane emergency braking method with theoretical analysis and experimental verification," *Nonlinear Dyn.*, vol. 98, no. 3, pp. 2211–2225, Nov. 2019.
[30] M. Zhang, Y. Zhang, B. Ji, C. Ma, and X. Cheng, "Modeling and energy-based sway reduction control for tower crane systems with double-pendulum and spherical-pendulum effects," *Meas. Control*, vol. 53, nos. 1–2, pp. 141–150, Jan. 2019.
[31] Y. Sun, J. Xu, H. Qiang, and G. Lin, "Adaptive neural-fuzzy robust position control scheme for Maglev train systems with experimental verification," *IEEE Trans. Ind. Electron.*, vol. 66, no. 11, pp. 8589–8599, Nov. 2019.
[32] J. Godjevac, "Comparison between PID and fuzzy control," LAMI IN F EPFL Ecublens, Vaud, Switzerland, Internal Rep. R93.36I, 1993.
[33] M. Esfandyari, M. A. Fanaei, and H. Zohreie, "Adaptive fuzzy tuning of PID controllers," *Neural Comput. Appl.*, vol. 23, no. S1, pp. 19–28, Dec. 2013.
[34] H. Bouadi, M. Bouchoucha, and M. Tadjine, "Modelling and stabilizing control laws design based on backstepping for an UAV type-quadrotor," *IFAC Proc. Volumes*, vol. 40, no. 15, pp. 245–250, 2007.
[35] S. Spedicato and G. Notarstefano, "Minimum-time trajectory generation for quadrotors in constrained environments," *IEEE Trans. Control Syst. Technol.*, vol. 26, no. 4, pp. 1335–1344, Jul. 2018.
[36] J. Vanualailai, B. Sharma, and S.-I. Nakagiri, "An asymptotically stable collision-avoidance system," *Int. J. Non-Linear Mech.*, vol. 43, no. 9, pp. 925–932, Nov. 2008.
[37] B. Sharma, J. Vanualailai, and U. Chand, "Flocking of multi-agents in constrained environments," *Eur. J. Pure Appl. Math.*, vol. 2, no. 3, pp. 401–425, 2009.
[38] T. Yoshizawa, "Asymptotic behavior of solutions of a system of differential equations," *Contrib. Differ. Equ.*, vol. 1, no. 3, pp. 371–387, 1963.
[39] T. Burton, *Volterra Integral and Differential Equations* (Mathematics in Science and Engineering). New York, NY, USA: Academic, 1983.
[40] J. Vanualailai, "Stable emergent formations for a swarm of autonomous car-like vehicles," *Int. J. Adv. Robot. Syst.*, vol. 16, no. 5, Sep. 2019, Art. no. 172988141984978.

JAI RAJ received the B.Sc. and M.Sc. degrees from The University of the South Pacific, Suva, Fiji, in 2009 and 2012, respectively, where he is currently pursuing the Ph.D. degree in control science, with the specific interest in the motion planning and control of unmanned aerial vehicles. He has worked in various roles, including as a tutor, a teaching, and a learning specialist. His research interests include stability of nonlinear systems, quadrotor unmanned vehicles, multiagent systems, robust nonlinear control, and swarming.

KRISHNA S. RAGHUWAIYA received the Ph.D. degree in cooperative control of swarm systems from The University of the South Pacific, Suva, Fiji, in 2017. In 2005, he joined as an Assistant Lecturer with the School of Computing, Information, and Mathematical Sciences, The University of the South Pacific, where he is currently a Senior Lecturer with the School of Education. His research interests include stability of nonlinear systems, volterra integro-differential systems, swarm intelligence, and mathematics education.

JITO VANUALAILAI received the Ph.D. degree in stability analysis of nonlinear systems from Kobe University, Japan, in 1994. He joined as a Lecturer in mathematics with The University of the South Pacific, Fiji, where he is currently a Professor of applied mathematics and the Director of Research. His research interests include stability of nonlinear systems, artificial neural networks, volterra integro-differential systems, planning algorithms, and swarm intelligence.